LOCALIZED HYDROGEN ANALYSIS IN SIMULATED GRAIN BOUNDARIES OF ALUMINUM ALLOYS EXPOSED TO STRESS CORROSION

RE-551

Final Report
(28 April 1975 to 28 September 1976)

February 1978

by

Philip N. Adler

Prepared Under Contract N00019-75-C-0394

for

Department of the Navy
Naval Air Systems Command
Washington, D.C. 20361

by

Research Department
Grumman Aerospace Corporation
Bethpage, New York 11714

Approved For Public Release;
Distribution Unlimited

LOCALIZED HYDROGEN ANALYSIS IN SIMULATED GRAIN BOUNDARIES OF ALUMINUM ALLOYS EXPOSED TO STRESS CORROSION.

(14) RE-551

(9) Final Report.

28 April 1975 to 28 September 1976

(11) February 1978 (12) 58 pp.

(15) Prepared Under Contract N00019-75-C-0394

for

Department of the Navy
Naval Air Systems Command
Washington, D.C. 20361

by

(10) Philip N. Adler
Research Department
Grumman Aerospace Corporation
Bethpage, New York 11714

Approved by: Richard A. Scheuing
Richard A. Scheuing
Director of Research

(11)
40 6 165

AB

UNCLASSIFIED

SECURITY CLASSIFICATION OF THIS PAGE (When Data Entered)

REPORT DOCUMENTATION PAGE

READ INSTRUCTIONS BEFORE COMPLETING FORM

1. REPORT NUMBER: RE- 551 ✓	2. GOVT ACCESSION NO.
3. RECIPIENT'S CATALOG NUMBER	
4. TITLE (and Subtitle): Localized Hydrogen Analysis In Simulated Grain Boundaries of Aluminum Alloys Exposed to Stress Corrosion	5. TYPE OF REPORT & PERIOD COVERED: Final Report 28 April 1975-28 Sept. 1976
	6. PERFORMING ORG. REPORT NUMBER: RE-551
7. AUTHOR(s): Philip N. Adler	8. CONTRACT OR GRANT NUMBER(s): N00019-75-C-0394 NAW
9. PERFORMING ORGANIZATION NAME AND ADDRESS: Research Department ✓ Grumman Aerospace Corporation Bethpage, New York 11714	10. PROGRAM ELEMENT, PROJECT, TASK AREA & WORK UNIT NUMBERS
11. CONTROLLING OFFICE NAME AND ADDRESS: Department of the Navy Naval Air Systems Command Washington, D.C. 20361	12. REPORT DATE: February 1978
	13. NUMBER OF PAGES
14. MONITORING AGENCY NAME & ADDRESS (if different from Controlling Office)	15. SECURITY CLASS. (of this report): UNCLASSIFIED
	15a. DECLASSIFICATION/DOWNGRADING SCHEDULE

16. DISTRIBUTION STATEMENT (of this Report)

Approved for Public Release; Distribution Unlimited

17. DISTRIBUTION STATEMENT (of the abstract entered in Block 20, if different from Report)

18. SUPPLEMENTARY NOTES

19. KEY WORDS (Continue on reverse side if necessary and identify by block number)

Aluminum
Stress Corrosion
Hydrogen Embrittlement

20. ABSTRACT (Continue on reverse side if necessary and identify by block number)

The role of hydrogen in the stress corrosion attack of 7000 series aluminum alloys was investigated using sputtered film/substrate samples to simulate the grain boundary constituents in these alloys. Localized hydrogen measurements were made in the film, interface region, and substrate using the Lithium Nuclear Microprobe for Hydrogen (LNMH) technique. Hydrogen concentrations were measured in samples of pure aluminum film/7075 substrate, 7475 film/7075 substrate, and $MgZn_2$ film/7075 substrate for as-sputtered, corrosion exposed, and stress corrosion exposed conditions as well as after stress

DD FORM 1 JAN 73 1473 EDITION OF 1 NOV 65 IS OBSOLETE
S/N 0102-014-6601

UNCLASSIFIED
SECURITY CLASSIFICATION OF THIS PAGE (When Data Entered)

#20 continued

removal. A substantial hydrogen concentration increase was observed in the interface region of $MgZn_2$ film/7075 substrate samples exposed to stress corrosion; smaller increases were introduced in the interface region of 7475 film/7075 substrate samples; no increase occurred in aluminum film/7075 substrate samples. The increase in hydrogen concentration was found to be stress dependent. Upon removal of stress, hydrogen was reduced to its initial concentration in the 7475 film/7075 substrate interface but remained trapped in the $MgZn_2$ film/7075 substrate interface. The relatively strong affinity for hydrogen in the interface region of $MgZn_2$ film/7075 substrate samples during stress corrosion exposure coupled with the actual stress corrosion failure of two of these samples suggest that stress corrosion attack in 7000 series aluminum alloys is hydrogen related.

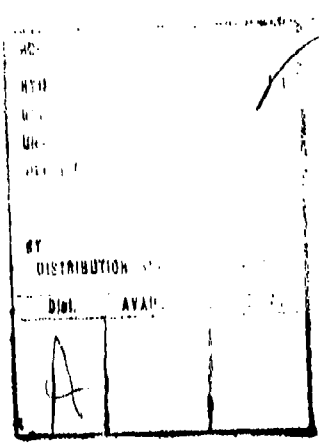

ACKNOWLEDGMENTS

A major impetus for this work was supplied by Mr. Sam Goldberg of the Naval Air Systems Command (AIR 52031), who over the past several years has actively supported the development and application of the Lithium Nuclear Microprobe for Hydrogen (LNMH) technique. The helpful suggestions and review of this work by Mr. E. Balmuth of the Naval Air System Command (AIR 52031G) are gratefully acknowledged.

Many people in the Grumman Research Department contributed to this program:

Dr. E. A. Kamykowski participated in the LNMH measurements and was responsible for the data analysis. Drs. G. M. Padawer, E. J. Schneid, R. L. Schulte, and G. Geschwind as well as F. J. Kuehne, Jr., J. R. Kennedy, and F. Ogilvie also participated in the LNMH measurements; Dr. G. M. Padawer suggested and conducted the nuclear measurements of film thickness; W. Poit, Jr. prepared and helped characterize the samples; C. Creter performed SEM and EDAX analysis; W. Poit, Jr., R. Squires, and C. Clamser helped design the special test device; and Drs. G. Geschwind, R. DeIasi, M. Russak, E. Schneid and G. M. Padawer contributed valuable discussions throughout the course of this work.

The staff of the Nuclear Structure Laboratory of SUNY at Stony Brook were of great help in maintaining operation of the accelerator facility during the LNMH measurements.

ABSTRACT

The role of hydrogen in the stress corrosion attack of 7000 series aluminum alloys was investigated using sputtered film/substrate samples to simulate the grain boundary constituents in these alloys. Localized hydrogen measurements were made in the film, interface region, and substrate using the Lithium Nuclear Microprobe for Hydrogen (LNMH) technique. Hydrogen concentrations were measured in samples of pure aluminum film/7075 substrate, 7475 film/7075 substrate, and $MgZn_2$ film/7075 substrate for as-sputtered, corrosion exposed, and stress corrosion exposed conditions as well as after stress removal. A substantial hydrogen concentration increase was observed in the interface region of $MgZn_2$ film/7075 substrate samples exposed to stress corrosion; smaller increases were introduced in the interface region of 7475 film/7075 substrate samples; no increase occurred in aluminum film/7075 substrate samples. The increase in hydrogen concentration was found to be stress dependent. Upon removal of stress, hydrogen was reduced to its initial concentration in the 7475 film/7075 substrate interface but remained trapped in the $MgZn_2$ film/7075 substrate interface. The relatively strong affinity for hydrogen in the interface region of $MgZn_2$ film/7075 substrate samples during stress corrosion exposure coupled with the actual stress corrosion failure of two of these samples suggest that stress corrosion attack in 7000 series aluminum alloys is hydrogen related.

TABLE OF CONTENTS

LIST OF ILLUSTRATIONS

LIST OF TABLES

1. INTRODUCTION

Stress corrosion is one of the most serious problems encountered with high-strength aluminum alloys of the Al-Zn-Mg type (Refs. 1 and 2). To avoid this problem, these alloys are used in a lower strength, overaged temper (Refs. 3 and 4). If the full strength capabilities of Al-Zn-Mg type alloys are to be realized, greater understanding of the mechanism of stress corrosion attack must be attained.

Recent evidence suggests that stress corrosion in these alloys is a form of hydrogen embrittlement. Speidel has shown that stress corrosion crack growth of 7079-T651 aluminum alloy in an aqueous salt environment is temperature dependent, with an activation energy for subcritical crack growth comparable to that observed in the embrittlement of nickel and iron-base alloys in distilled water (Ref. 5). Speidel suggests that similar rate controlling steps for hydrogen entry are involved in all these material environment combinations. Green, Hayden, and Montague have found that stress corrosion cracking susceptibility of 7075-T6 aluminum alloy is far greater under tensile (mode I) loading than torsional (mode III) loading (Ref. 6). They conclude that under torsion loading the component of hydrostatic stress is insufficient to cause a concentration of hydrogen ahead of the crack tip whereas hydrogen damage is a dominant mechanism leading to stress corrosion failure under tensile loading.

Another indication that hydrogen is an important factor in stress corrosion attack concerns the effect of pre-exposure. Gruhl and Brungs have found that uncracked specimens of Al-Zn-Mg alloy exhibited a reduction from 20 to 13 percent elongation

after stress corrosion exposure in an aqueous chloride environment (Ref. 7). These specimens showed evidence of intergranular attack after testing. However, if exposed samples were reheat-treated to their original temper, no ductility loss was observed. The loss in ductility was interpreted as grain boundary embrittlement by hydrogen that was eliminated in subsequent heat treatment.

In direct observations of stress corrosion attack using transmission electron microscopy, Montgrain and Swann exposed an Al-7% Zn-3%Mg alloy to a saturated water vapor environment. They found that intergranular crack propagation takes place at the interface between incoherent $MgZn_2$ grain boundary precipitates and one of the grains (Ref. 8). No evidence of grain boundary precipitate dissolution was observed during crack propagation but evolution of molecular hydrogen was measured during deformation and fracture.

One of the major arguments against a hydrogen-related mechanism of stress corrosion attack in high strength aluminum alloys has been that cathodic polarization acts to reduce stress corrosion attack. Since copious amounts of hydrogen exist at the cathode, one would expect enhanced attack if hydrogen was significant to the attack mode. However, recent work of Gest and Troiano (Ref. 9) show that hydrogen permeability in 7075-T651 in a 3 percent NaCl solution goes through a minimum over the -800 to -1200 mV applied potential range (relative to Standard Calomel Electrode). Since the open circuit potential is approximately -800 mV, hydrogen would be relatively immobile until cathodic potentials in excess of -1200 mV were applied. Indeed, Gest and Troiano found a significant increase in stress corrosion crack growth velocity at an applied potential of -1500 mV.

Although the studies described above strongly suggest that stress corrosion attack in Al-Zn-Mg type alloys is related to hydrogen embrittlement, other mechanisms have been more generally accepted, and the role of hydrogen is considered quite controversial (Ref. 10). The purpose of the present work is to clarify the role of hydrogen in the intergranular attack mode characteristic of stress corrosion in these alloys by direct measure of the hydrogen concentration in simulated grain boundary regions exposed to stress corrosion. Previous work has shown the importance of the grain boundary precipitate in stress corrosion attack (Refs. 8, 11-15). In the present work, localized hydrogen concentration was measured using the recently developed Lithium Nuclear Microprobe for Hydrogen (LNMH) technique that has a depth resolution of approximately ±0.10 μm in the materials studied (Refs. 16-18). To capitalize on this depth resolution capability, a film/substrate sample configuration was utilized for the grain boundary simulation. In this configuration, the constituents at a grain boundary are represented by the film and substrate, with the interface that separates the film and substrate representing the grain boundary. Hydrogen concentrations were measured in the film, interface, and substrate regions of samples exposed to corrosion and stress corrosion environments as well as in control samples.

2. EXPERIMENTAL

LOCALIZED HYDROGEN ANALYSIS

For this study, the LNMH technique was utilized to determine localized hydrogen concentrations. This technique is based on measuring the characteristic 14.7- and 17.6-MeV gamma rays emitted during the resonant $^{1}H(^{7}Li,\gamma)^{8}Be$ nuclear reaction, as illustrated in Fig. 1. The gamma-ray yield is proportional to hydrogen concentration. In practice, ^{7}Li ions are accelerated in a Van de Graaff accelerator and allowed to strike a target sample. For accelerated ^{7}Li ions at the resonance energy for this reaction, 3.07 MeV, only the hydrogen atoms at the very outer surface of the sample will be measured. As the energy of the accelerated ^{7}Li ions is increased, the resonant reaction occurs at deeper lying regions below the surface via slowing down of the incident ^{7}Li ions to the resonance energy. Thus, hydrogen concentration depth profiles can be measured by varying the accelerator voltage. Since the resonance width is very narrow (0.08 MeV), the depth resolution of the LNMH for metals is typically ±0.05 to ±0.15 μm, depending on sample composition. For the aluminum and $MgZn_2$ samples herein studied, the depth resolution is approximately ±0.10 μm.

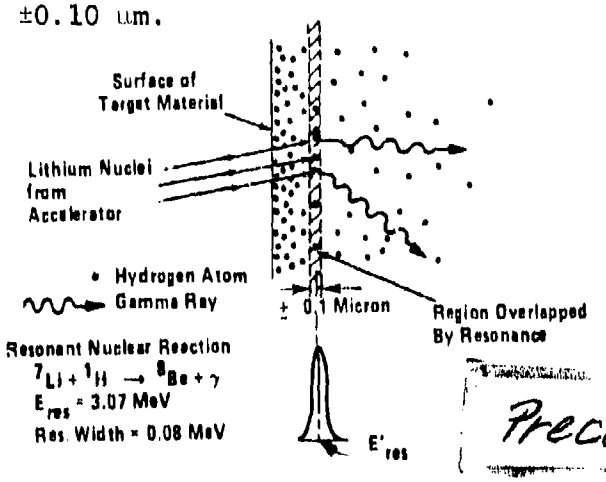

Fig. 1 LNMH Fundamentals

Localized hydrogen analysis with the LNMH can be done effectively using the depth resolution capability of this approach. For study of hydrogen concentration at grain boundary regions associated with stress corrosion exposure, the film/substrate sample configuration illustrated in Fig. 2 was utilized. This sample configuration enabled simulation of the chemical constituents typical of the grain boundary in Al-Zn-Mg type alloys and permitted depth profiling in the film, interface, and substrate regions. By in situ measurements in these regions, hydrogen concentrations associated with different conditions of environment exposure were determined.

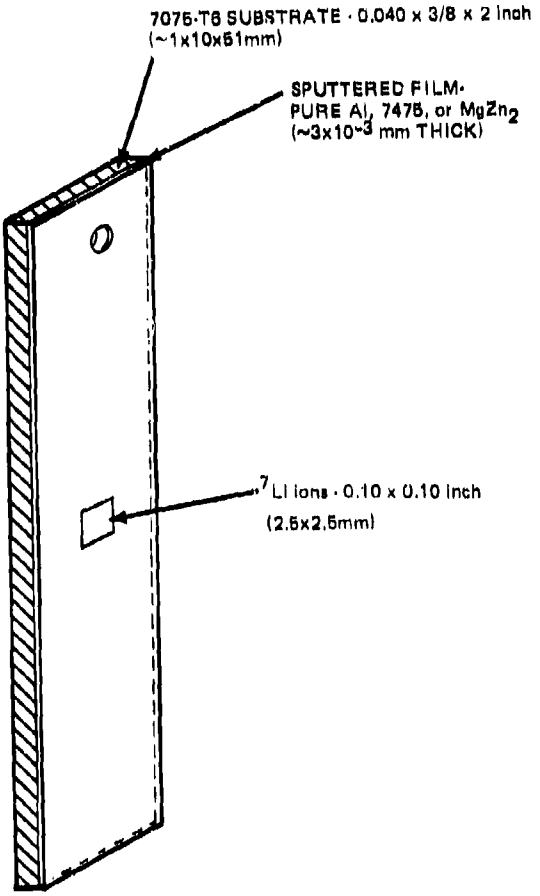

Fig.2 Schematic of Film/Substrate Sample

SAMPLE PREPARATION

Samples were prepared by sputtering specific films onto 7075-T651 aluminum alloy substrates. Films of pure aluminum, 7475 aluminum alloy, and $MgZn_2$ were sputtered from appropriate targets. The pure aluminum target was zone-refined material having a nominal purity of 99.999+%; the 7475 aluminum alloy target was prepared from 3/16-inch thick plate that contained 5.60 wt% Zn, 2.44% Mg, 1.43% Cu, and less than 0.01% of Cr, Fe, Si, Mn or Ti; the $MgZn_2$ target was prepared from vacuum-hot-pressed powder that contained no binders. These targets were assembled by the Materials Research Corporation (MRC). The 7475 aluminum alloy is a high purity form of 7075 that was specially supplied by the Metallurgical Research Division of the Reynolds Metals Company. Substrates, of 0.040-inch thickness x 3/8-inch width x 2-inch length, were sliced from 3-inch thick 7075-T651 bar stock; the 2-inch substrate length was in the short transverse direction of the bar. These substrates were polished to a 0.065 ± 0.015 μm rms finish (as measured with a profilometer) using standard metallographic techniques and a 0.05 μm final grit size. Substrate polishing was utilized to avoid the surface roughness that was previously found to limit depth resolution capability in the interface region (Ref. 19). Prior to film deposition, substrates were sputter-etched to remove surface contaminants and promote adherence with the sputtered film.

Both sputter etching and film sputtering were done in a MRC Model SEM-8620 RF Sputter-Etch Unit. During preliminary experiments, relatively high hydrogen concentrations, of the order of 100 wppm, were measured by LNMH in pure aluminum sputtered films. Contamination introduced by the argon gas used in sputtering was suspected. Therefore, Research Grade Argon of 99.9995% purity, the

highest purity argon commercially available, was substituted for normally used High Purity Argon. In addition, the argon gas was purified by a titanium-getter heater prior to entry into the sputtering unit. These changes reduced the hydrogen concentration in the pure aluminum sputtered films is less than 40 wppm.

Another problem encountered during preliminary sputtering experiments concerned substrate softening caused by heating. A reduction in the yield strength of 7075-T651 substrates from 67 to 16 ksi was encountered. Such softening was undesirable since only minimal elastic loadings could be applied during stress corrosion exposure. Therefore different methods to avoid substrate heating during sputtering were evaluated. It was found that use of a high vacuum silicone grease on the back surface of the substrate served to enable sufficient heat transfer during sputtering to avoid softening. In fact, no change in substrate hardness was experienced when using the silicone grease. Therefore this procedure was used uniformly in preparing film/substrate samples.

FILM CHARACTERIZATION

Both gravimetric and nuclear resonance techniques were utilized in measuring the thickness and thickness uniformity of sputtered films. Scanning Electron Microscopy (SEM) and X-ray diffraction were also used for film characterization. Film surface topography was examined using an Advanced Metals Research Corporation (AMR) Model 1000 Scanning Electron Microscope (SEM). Films were examined after sputtering and each condition of environmental exposure. In conjunction with SEM examination, Energy Dispersive Analysis of X-Rays (EDAX) was used in identifying the elemental constituency in localized film regions. The crystallographic character of the sputtered films was measured using a Picker X-ray Diffractometer with a copper target.

Accurate measurement of film thickness was important in locating the interface region of each sample. Film thickness was determined by weight difference before and after sputtering. No significant substrate weight loss was measured for the sputter etching treatment utilized. Careful attention was paid to remove all the silicone high vacuum grease that was used to transfer heat from the substrate during sputtering. Before final weighing, each sample was cleaned in an ultrasonic bath of trichloroethylene for 1 min followed by successive 1 min rinses in separate ultrasonic baths of Freon. This procedure was effective since no further weight loss was observed by additional cleaning.

Film thickness will be expressed in units of mg/cm^2 throughout. When thickness is indicated in microns, a density value of 2.71 g/cm^3 has been used for the pure aluminum and 7475 films, and 5.20 g/cm^3, based on the density of crystalline material (Ref. 20), has been used for the $MgZn_2$ films. Since the samples contained a hole and were not of uniform width, an accurate measure of surface area was obtained for each substrate by dividing the substrate weight by the product of the thickness and density. Substrates were 0.038 ± 0.002-inch thick and were measured to the nearest 0.001 inch. Weighings were made to the nearest 0.01 mg. For the films prepared, weight increases were of the order of 4-6 mg. The overall error in the determination of film thickness is estimated as 3 percent and is primarily related to the precision in substrate thickness measurement.

In addition to the gravimetric approach, the thickness of selected sputtered films was measured using a nuclear technique based on stimulation of proton-induced resonances. This approach was used to corroborate gravimetric measurements and provide a means of evaluating the uniformity of film thickness over an

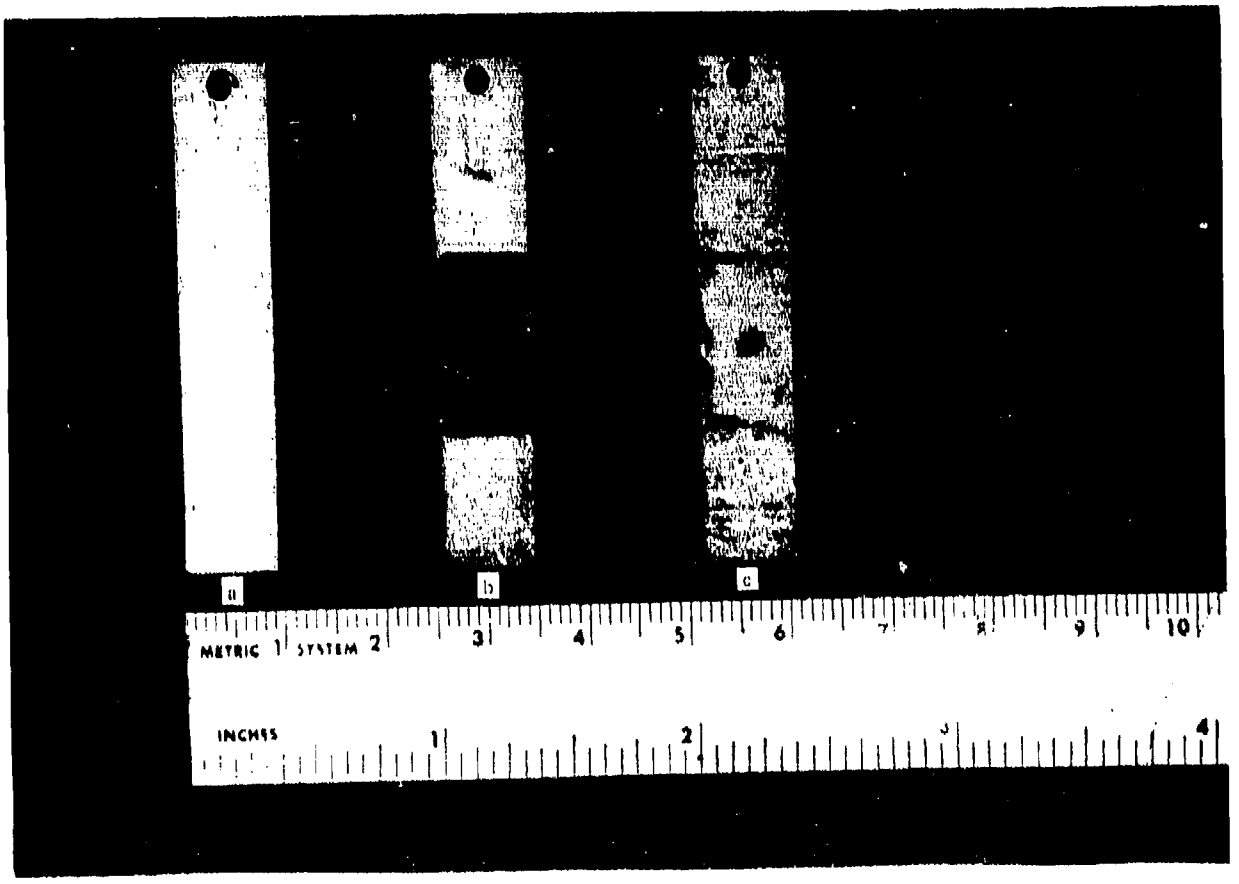

Fig. 3 Sample Surface Masking
(a) As-Sputtered Sample
(b) Masked Sample Before Environmental Exposure
(c) Sample After Environmental Exposure and LNMH Measurement

area equivalent to that used with the LNMH. Two variations of the technique were necessary. For $MgZn_2$ films, the resonance reaction between fast protons and aluminum nuclei in the substrate, $^{27}Al(p,\gamma)^{28}Si$ at E_{res} = 0.992 MeV, was utilized. For pure aluminum and 7475 aluminum alloy films, the small aluminum composition difference between film and substrate made use of this reaction impracticable. Therefore, a surface "marker" consisting of a very thin layer of LiF was evaporated onto six selected polished 7075 substrates prior to sputtering, and the resonance reaction between fast protons and fluorine nuclei, $^{19}F(p,\alpha\gamma)^{16}O$ at E_{res} = 0.874 MeV, was utilized. Film thickness was calculated from the measured shift of resonance energy. The width of the resonance energy profile, corrected for natural line width, proton-beam energy dispersion, and straggling, provided a measure of the variation in film thickness within the 0.10 x 0.10-inch area probed.

ENVIRONMENTAL EXPOSURE

Samples of each film/substrate combination were exposed to a corrosion or stress corrosion environment at room temperature prior to the LNMH measurement. An aqueous chloride solution containing 3 percent NaCl and 0.5 percent $AlCl_3.6H_2O$ and having a 3.5 pH was used as the corrosion medium. The solution was constantly stirred during the 500 min exposure time. Earlier, it had been found that a corrosion product at least 3 μm thick formed during similar environmental exposure (Refs. 16, 18). Formation of such a corrosion product would obscure desired LNMH measurements. Therefore, masking was used to prevent contact between the solution and film surface region to be probed. Masking consisted of a combination of an inner 0.200-inch x 1/2-inch Teflon tape, an outer 0.300-inch x 3/4-inch electrical insulating tape seal, and a perimeter seal of Collodion. The

masks were placed over the center portion of the sample film surface as shown in Fig. 3, and were removed before LNMH measurement.

A test device was designed and built for stress corrosion exposure. The device, shown in Fig. 4, was capable of accommodating eight samples (five are shown in Fig. 4). Stress was applied using four-point bending and was maintained during exposure and subsequent LNMH measurement. The inner-two loading points were specific to each sample and are shown at the three unoccupied sample positions in Fig. 4; the outer-two loading points were continuous near the top and bottom of the device. By displacement of the inner contact points, a constant elastic stress was produced on the sample in the 1/2-inch length between inner contacts. Two devices were fabricated and used for both stress corrosion and corrosion exposures as well as for holding samples during the LNMH measurements. The devices were machined from 321 stainless steel plate and were coated with an epoxy fuel tank paint to avoid galvanic interaction with the samples. The strain-displacement characteristics of each sample position was calibrated using an SR-4 strain gage on the outer sample surface. Each position was found to be independent of the loading on other samples. Based on repeated strain measurements and a 10.4×10^6 psi elastic modulus, known displacements resulted in an average deviation of $\pm$ 4.5% to 60 ksi.

Samples were stress corrosion exposed under either an elastic or plastic strain in the substrate surface. For elastic loading, a stress of 29 ksi was applied; for plastic loading, the stress was 64 ksi. The latter value is based on an applied strain of 0.675 percent and the stress strain behavior of the 7075 aluminum alloy substrate. For $MgZn_2$ films at this

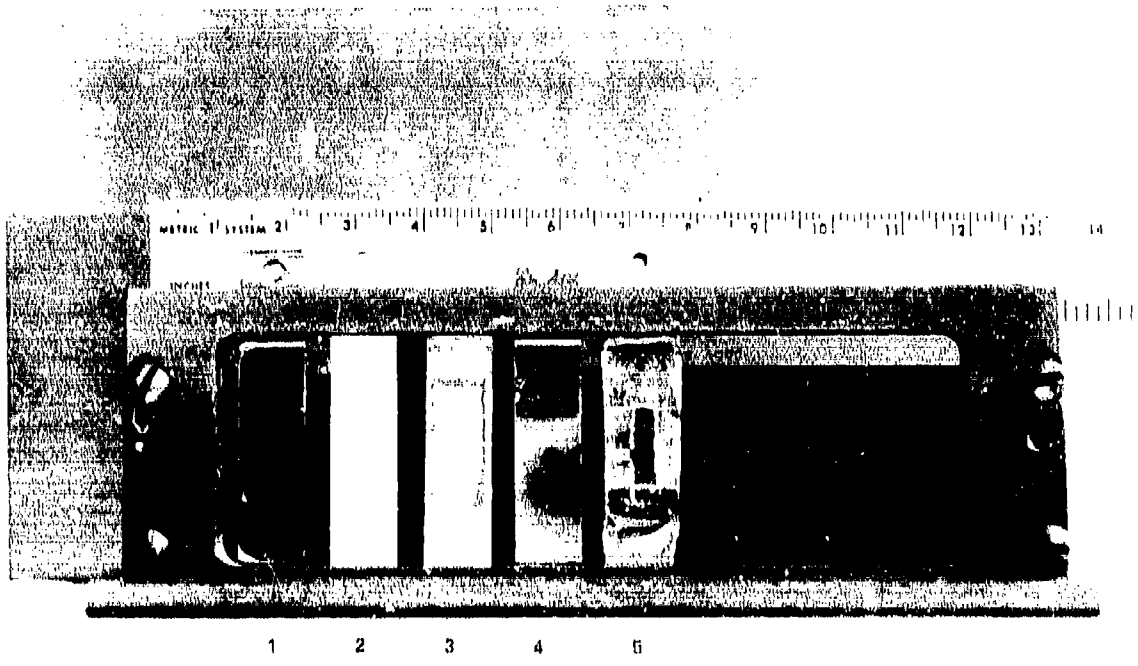

Fig. 4 Test Device for Loading and Environmental Exposure. Five Sample Positions are Occupied:

1 - Sputter-Etched Substrate
2 - As-Sputtered Al Film/Substrate Sample
3 - Corrosion Exposed Al Film/Substrate Sample
4 - Stress Corrosion Exposed (Plastic-Loading) 7475 Film/Substrate Sample
5 - Stress Corrosion Exposed (Plastic-Loading) $MgZn_2$ Film/Substrate Sample with Partial Al Overlay Mask

strain, the stress was approximately 74 ksi since both aluminum and $MgZn_2$ have almost the same modulus (Ref. 21) and $MgZn_2$ would not be expected to undergo plastic deformation.

LNMH MEASUREMENTS

Hydrogen concentration was measured in the film, interface, and substrate regions of unexposed and exposed film/substrate samples as well as in the surface of polished and sputter etched substrates. LNMH measurements were made at the Nuclear Structure Laboratory, SUNY, Stony Brook, New York using the doubly ionized ^7Li beam of a High Voltage Engineering Corporation (HVEC) Model FN Tandem Van de Graaff Accelerator. To facilitate measurements in the numerous samples examined, ^7Li beam energies of 4.25, 4.75, and 5.25 MeV were utilized to examine the film, interface and substrate regions, respectively, and samples of specific film thickness were prepared so that the LNMH resonance reaction occurred in the interface region at a 4.75 MeV beam energy. The actual depths of the LNMN measurement are given in Table 1 and are based on accurately known stopping powers for the elemental constituency of the sample (Ref. 22).

Hydrogen concentrations were measured in two samples of each film/substrate type for each of the following conditions:

As-Sputtered (S)
Corrosion Exposed (C)
Stress Corrosion Under Elastic Stress (SCE)
Above With Stress Removed (SCE-U)
Stress Corrosion Under Plastic Stress (SCP)
Above With Stress Removed (SCP-U)

One as-polished and two sputter etched substrates were also examined at the 4.25, 4.75 and 5.25 MeV energies. LNMH measurements

TABLE 1 DEPTH OF LNMH MEASUREMENT

Sample (Film/Substrate)	Depth of Measurement†					
	4.25 MeV (Film)		4.75 MeV (Interface)		5.25 MeV (Substrate)	
	mg/cm^2	μm‡	mg/cm^2	μm‡	mg/cm^2	μm‡
Pure Al/7075	0.61	2.25	0.91±0.03	3.36±0.11	1.23	4.54
7475/7075	0.61	2.25	0.91±0.03	3.36±0.11	1.23	4.54
$MgZn_2$/7075	0.95	1.63	1.25±0.05	2.40±0.09	1.58	3.58

† Deviations are based on LNMH reaction resonance width and straggling and are approximately the same at the three energies investigated.

‡ Based on density of 2.71 g/cm^3 for Al, 7075 and 7475 and 5.20 g/cm^3 for $MgZn_2$.

were made 19 ± 1 days after environmental exposure. One of the $MgZn_2$ film/substrate samples exposed to SCP failed while under load less than one day after being removed from the solution environment. This sample was examined in the unloaded condition (SCP-U), and a third $MgZn_2$ film/substrate SCE sample was substituted. (During preliminary exposure evaluation, a similar failure occurred in another $MgZn_2$ film/substrate sample exposed under SCP shortly after removal from the solution environment.) These were the only two sample failures that were encountered during the course of this investigation.

A 0.10 x 0.10-inch beam collimator was used throughout. The area examined was always within the inner-two contact points of the test device. Alignment for the different sample positions of

the test device relative to the ^{7}Li beam was established prior to LNMH measurement. A cathetometer was used to align the beam collimator with a reference cross-hair on the LNMH target chamber. The test device was mounted on a X-Y positioning stage within the target chamber and specific positions were indexed at the areas to be measured. Insertion of the X-Y positioning stage into the LNMH target chamber is shown in Fig. 5. Although surface masking during solution exposure was generally effective in preventing corrosion product formation on the film area to be examined, a limited number of samples did undergo attack near their edges. For these cases, a partial overlay mask of pure aluminum sheet was used to eliminate any possibility of interaction between the corrosion product and the ^{7}Li beam. (A sample with an overlay mask as well as four unmasked samples, are shown after LNMH measurement in Fig. 4. The area probed with the beam is evidenced by the darkened "beam spot".)

A total of 40 samples were examined in five separate target chamber loadings (eight samples per loading). For each sample, measurement was made at three depths, so that in total, 120 LNMH measurements were made. A specially prepared NBS 354 H-in-Ti Standard, 215 ± 6 wppm, (Ref. 16) was used for calibrating each loading at each of the three energies examined. A vacuum annealed pure iron standard was also examined periodically as a measure of beam-dependent-background. Beam currents from 70-190 na were used and were generally in the 130-150 na range. Measurement times were of the order of 400-800 sec depending on the hydrogen concentration being measured and the desired count statistics. Measurement times were subdivided into equivalent charge collection periods to monitor possible time dependent concentration change during the measurement. In no case was

any time dependent concentration change observed for the range of beam currents utilized. Each sample loading required approximately 9 hours of measurement time.

In addition to LNMH measurements at 4.25, 4.75 and 5.25 MeV, hydrogen concentration-depth profiling was done in the surface of polished and sputter-etched substrates over the 3.08 to 3.85 MeV energy range. Surface profiling was done at Grumman's 4 MV Van de Graaff Accelerator facility using singly ionized ^{7}Li.

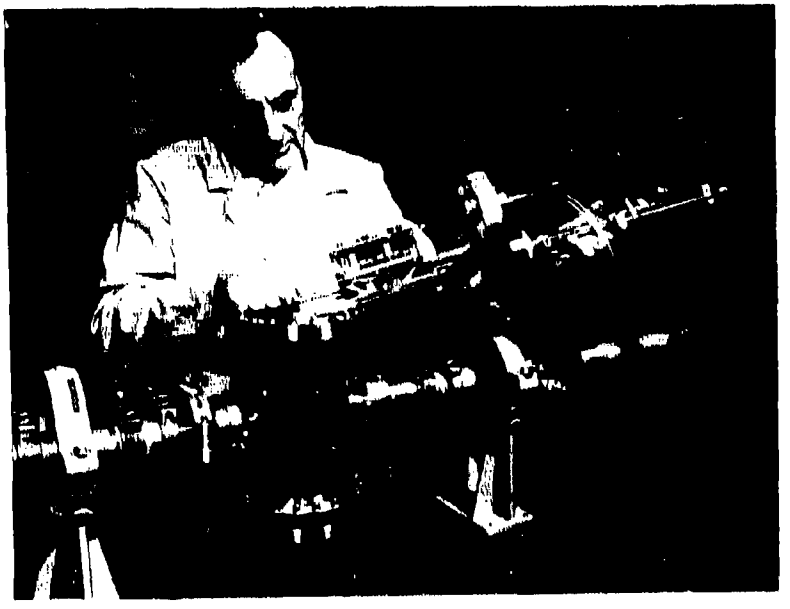

Fig. 5 LNMH Target Chamber Assembly. Test Device is Mounted on X-Y Positioning Stage

3. RESULTS AND DISCUSSION

FILM DESCRIPTION

Accurate measurement of film thickness was important to establish the depth at which the film/substrate interface was located in each sample. Film thickness was determined from the weight difference before and after sputtering and the substrate surface area. The accuracy of this gravimetric method was evaluated using a nuclear technique of film thickness measurement on selected samples. Comparison of film thickness results for specific film/substrate samples is made in Table 2. As indicated, the agreement between these two techniques is quite good.

TABLE 2 FILM THICKNESS MEASUREMENT COMPARISON

Film	Thickness (mg/cm^2)		
		Nuclear Method	
	Gravimetric Method	Average and Maximum Deviation†	Maximum Local Variation‡
Pure Aluminum	1.36 ± 0.02	1.28 ± 0.09	± 0.06
	1.25 ± 0.02	1.22 ± 0.09	± 0.06
	1.23 ± 0.02	1.16 ± 0.06	± 0.06
7475 Aluminum Alloy	1.48 ± 0.02	1.48 ± 0.01	± 0.05
	1.45 ± 0.02	1.43 ± 0.00	± 0.06
	1.50 ± 0.02	1.45 ± 0.01	± 0.06
$MgZn_2$	1.13 ± 0.02	1.10 ± 0.00	± 0.06

† Based on three to five separate areas in same sample

‡ Within 0.10 x 0.10 inch area — calculated from broadening of resonance width

Variation in film thickness within the 0.10 x 0.10-inch area probed was also determined from the nuclear measurements. Based on the extent of broadening in the resonance width of the $^{27}Al(p,\gamma)^{28}Si$ reaction for the $MgZn_2$/7075 sample and of the $^{19}F(p,\alpha\gamma)^{16}O$ reaction in the pure aluminum/7075 and 7475/7075 samples, the variation was $\pm$ 0.06 mg/cm^2, as indicated in Table 2. Since this variation is approximately three times larger than the precision of the average film thickness measured using the gravimetric method, an uncertainty of $\pm$ 0.06 mg/cm^2 will be used in describing sample film thickness.

Both X-ray diffraction and SEM were used in characterizing sputtered films. Initially, films were sputtered onto glass substrates to determine their crystalline nature as a function of film thickness. As indicated in Table 3, the films were crystalline with the exception of one $MgZn_2$ film of 0.17 mg/cm^2 thickness. Diffraction patterns could be indexed with expected lattice parameters and crystal structures (Ref. 20). These films generally had a preferred orientation that changed with film thickness.

Subsequently, films were sputtered onto 7075-T6 substrates. The topographies of these films are illustrated in the SEM micrographs of Fig. 6. Films of pure aluminum and 7475 aluminum alloy appear similar and have a cubic crystallite morphology with an approximate 3-6 μm size; crystallites of the $MgZn_2$ film have a spherical morphology and an approximate 0.5-2 μm size. Since the thickness of these films is of the order of 2-4 μm, it is likely that the films are a polycrystalline array only one or two crystals thick.

Use of high vacuum silicone grease on the back surface of each substrate during sputtering resulted in cooler substrates

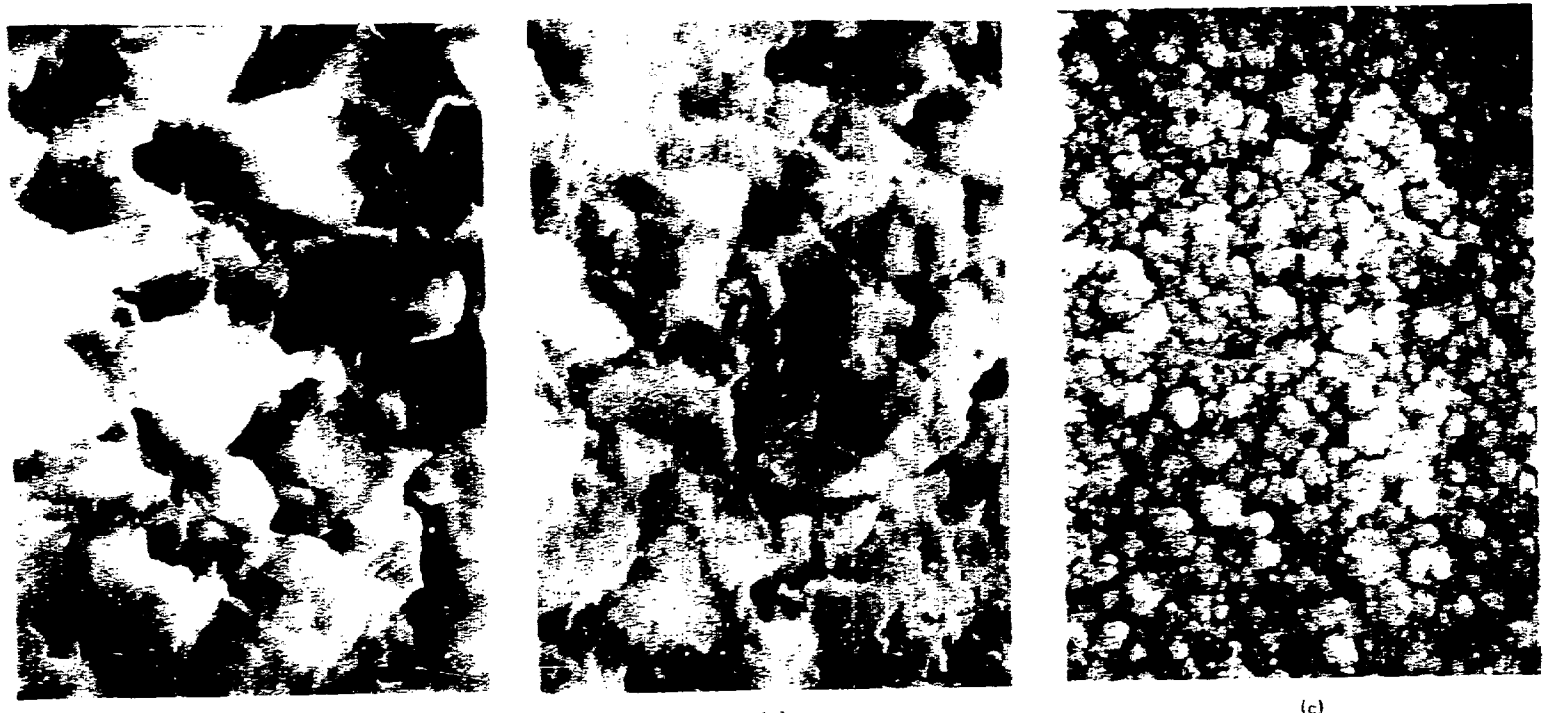

(a) (b) (c)

Fig. 6 Scanning Electron Micrographs of Sputtered Film Topography (on Softened Substrates) (3200x)
(a) Pure Aluminum Film 1.04 mg/cm^2 (3.8μm) Thick
(b) 7475 Aluminum Alloy Film 0.87 mg/cm^2 (3.2μm) Thick
(c) $MgZn_2$ Film 1.05 mg/cm^2 (2.0μm) Thick

TABLE 3 SPUTTERED FILM CRYSTALLOGRAPHIC CHARACTERISTICS†

Film	Thickness		Crystallographic Nature‡
	(mg/cm^2)	(μm)#	
Pure Aluminum	1.17	4.32	FCC*
7475 Aluminum Alloy	0.10	0.37	FCC, Fine Grained
	0.17	0.63	FCC
	0.42	1.6	FCC, {200}
	0.99	3.7	FCC, {200}
$MgZn_2$	0.17	0.33	Amorphous
	0.65	1.3	HCP, *{10·0}
	0.92	1.8	HCP, {10·0}
	1.83	3.52	HCP, {00·2}
	14.4	27.7	HCP, {00·2}

† Sputtered onto glass substrate

‡ Based on a density of 2.71 g/cm^3 for the aluminum and 7475 films, and 5.20 g/cm^3 for $MgZn_2$ film

Planes of preferred orientation indicated where observed

* FCC - Face Centered Cubic
HCP - Hexagonal Close Packed

that significantly affected the crystallographic nature of the sputtered films. For pure aluminum, the crystallite morphology remained comparable to that on hotter substrates, but the size of the cubic crystallites was reduced from 4-6 μm to approximately 0.8 μm. The crystallite morphology of the 7475 aluminum alloy film was difficult to discern but appeared less cubic than on hotter substrates, and crystallite size was reduced from 3-6 μm

to approximately 0.5 μm. No discrete crystalline morphology was apparent in the topography of sputtered $MgZn_2$ films. X-ray diffraction results substantiated the crystalline nature of the pure aluminum and 7475 aluminum alloy films but indicated that the $MgZn_2$ films were amorphous. Diffraction patterns from the pure aluminum and 7475 film/substrate samples differed from those of the 7075-T6 substrate in the relative intensity of {311} planes. To corroborate the crystalline nature of the pure aluminum and 7475 aluminum alloy films, these films were sputtered onto cooled copper substrates. In both cases, diffraction results showed the films to be crystalline. Diffraction results from $MgZn_2$ film/substrate samples, however, exhibited none of the peaks observed from films sputtered onto hotter substrates. Extensive broadening, extending over 9-10°, was apparent over ranges of 2θ where three or more diffraction peaks had been observed in crystalline films. Therefore, it can be concluded that only short range ordering existed in the $MgZn_2$ films that were sputtered onto the cooler substrates.

LOCALIZED HYDROGEN MEASUREMENTS

Results of LNMH measurements in as-polished and sputter etched substrates at depths of 0.61, 0.91 and 1.23 mg/cm^2 (4.25, 4.75, and 5.25 MeV energies, respectively) were below the limit of detectability, 19 wppm, used for these measurements. Longer measurement times or increased beam currents would have been required to reduce the detectability limit further, and this was not considered necessary for the scope of the present work. These samples were examined in different target chamber

loadings, and the low hydrogen concentrations, consistent with earlier work (Ref. 16), attest to the absence of background problems throughout these measurements.

The hydrogen concentration results for each of the film/substrate combinations are summarized in Tables 4, 5, and 6. Hydrogen concentrations in individual samples are indicated for the film, interface region, and substrate for the different conditions of exposure. For pure aluminum film/substrate samples, see Table 4, the hydrogen concentrations in the film and substrate are generally below the limit of detectability used for these samples. The low concentrations measured in the film are indicative of an absence of surface contamination and of relatively little hydrogen trapping during sputtering; the low concentrations in the substrate are as expected for bulk 7075 aluminum alloy and confirm that no contamination problem existed in any of these samples. High hydrogen concentrations exist in the interface region for all conditions examined, but no significant increases appear to be associated with stress corrosion exposure. In fact, the disparity in concentration for a specific condition is comparable to the total range of concentrations observed, i.e., as-sputtered samples have interface concentrations of 121 ± 20 and 230 ± 32 wppm, and the total range of hydrogen concentrations measured for this group of samples is 85 to 230 wppm.

For 7475 film/substrate samples, see Table 5, the hydrogen concentration in the substrates is below the limit of detectability; the alloy films have measurable concentrations that are higher than those observed in the pure aluminum films. These higher concentrations are likely a result of hydrogen trapping

TABLE 4 HYDROGEN CONCENTRATION IN ALUMINUM FILM/SUBSTRATE SAMPLES

Condition	Hydrogen Concentration (wppm)		
	Aluminum Film*[1]	Interface Region*[2]	7075 Substrate*[3]
As-Sputtered (S)	<39 <39	121 ± 20 230 ± 32	<37 <24
Corrosion Exposure (C)	<39 <39	116 ± 20 85 ± 18	<31 <24
Stress Corrosion Elastic*[4] (SCE)	50 ± 16 <40	189 ± 25 169 ± 24	<30 <19
Unloaded SCE (SCE-U)	<39 <36	155 ± 23 137 ± 22	67 ± 17 <37
Stress Corrosion Plastic*[5] (SCP)	<38 ---	229 ± 28 123 ± 21	<26 <40
Unloaded SCP (SCP-U)	<32 60 ± 15	108 ± 17 102 ± 19	<28 <19

*[1] Depth of 0.61 mg/cm^2 (2.25μm) below surface

*[2] Depth of 0.91 mg/cm^2 (3.36μm) below surface

*[3] Depth of 1.22 mg/cm^2 (4.50μm) below surface

*[4] Elastic stress of 29 ksi

*[5] Plastic stress of 64 ksi

TABLE 5 HYDROGEN CONCENTRATION IN 7475 FILM/ SUBSTRATE SAMPLES

Condition	Hydrogen Concentration (wppm)		
	7475 Film*[1]	Interface Region*[2]	7075 Substrate*[3]
As-Sputtered (S)	54 ± 15 90 ± 16	167 ± 23 68 ± 15	<19 <25
Corrosion Exposure (C)	44 ± 12 84 ± 16	199 ± 29 45 ± 13	<38 <38
Stress Corrosion Elastic*[4] (SCE)	52 ± 14 66 ± 17	192 ± 25 105 ± 19	<19 <26
Unloaded SCE (SCE-U)	<44 75 ± 16	145 ± 22 104 ± 19	<19 <35
Stress Corrosion Plastic *[5] (SCP)	67 ± 17 71 ± 15	248 ± 28 82 ± 17	<40 <19
Unloaded SCP (SCP-U)	72 ± 15 64 ± 15	162 ± 23 58 ± 16	<25 <23

*[1] Depth of 0.61 mg/cm^2 (2.25μm) below surface

*[2] Depth of 0.91 mg/cm^2 (3.36μm) below surface

*[3] Depth of 1.22 mg/cm^2 (4.50μm) below surface

*[4] Elastic stress of 29 ksi

*[5] Plastic stress of 64 ksi

TABLE 6 HYDROGEN CONCENTRATION IN $MgZn_2$ FILM/ SUBSTRATE SAMPLES

Condition	Hydrogen Concentration (wppm)		
	$MgZn_2$ Film*[1]	Interface Region*[2]	7075 Substrate*[3]
As-Sputtered (S)	26 ± 3 36 ± 5	214 ± 24 203 ± 24	<26 <38
Corrosion Exposure (C)	50 ± 6 39 ± 6	140 ± 20 101 ± 17	<38 <38
Stress Corrosion Elastic*[4] (SCE)	31 ± 4 47 ± 6 53 ± 6	274 ± 29 400 ± 41 170 ± 22	<40 54 ± 14 78 ± 17
Unloaded SCE (SCE-U)	30 ± 4 53 ± 6 58 ± 7	183 ± 23 457 ± 49 168 ± 22	<39 86 ± 18 64 ± 17
Stress Corrosion Plastic*[5] (SCP)	52 ± 6 ---	426 ± 47 ---	70 ± 17 ---
Unloaded SCP (SCP-U)	60 ± 7 48 ± 6	355 ± 38 538 ± 54	41 ± 15 71 ± 17

*[1] Depth of 0.85 mg/cm^2 (1.63μm) below surface

*[2] Depth of 1.25 mg/cm^2 (2.40μm) below surface

*[3] Depth of 1.56 mg/cm^2 (3.54μm) below surface

*[4] Elastic stress of 29 ksi

*[5] Plastic stress of 64 ksi

during sputtering and indicate that the alloy has a greater affinity for hydrogen than pure aluminum. High hydrogen concentrations exist in the interface region, and there appears to be some increase for specific exposure conditions.

For the $MgZn_2$ film/substrate samples, see Table 6, both film and substrates have comparatively low hydrogen concentrations; slightly higher concentrations exist in most of the substrates exposed to stress corrosion. In the interface region, there is clear indication that stress corrosion exposure, especially under plastic loading, leads to hydrogen enrichment. Only one of three samples has a significantly higher hydrogen concentration after exposure to stress corrosion under elastic loading, SCE, whereas both samples exposed under plastic loading, SCP, have exceptionally high hydrogen concentrations. For one of the SCP samples, failure occurred in a typical stress corrosion manner while stress was maintained before LNMH measurement. This is illustrated by the intergranular cracking and failure mode shown in Fig. 7.

For each of the previously described film/substrate samples, the hydrogen concentration in the interface region was much higher than in the film or substrate. Since the high concentrations exist in as-sputtered samples, they appear inherent to the interface region. To determine whether these high hydrogen concentrations could be attributed to a substrate surface condition, hydrogen concentration depth profiling was done in the surface of as-polished and sputter-etched substrates. These profiles, which are shown in Fig. 8, clearly indicate that the hydrogen concentration within the first 0.20 μm of the substrate is well in excess of 100 wppm. Since the resonance width for the LNMH measurements at the interface

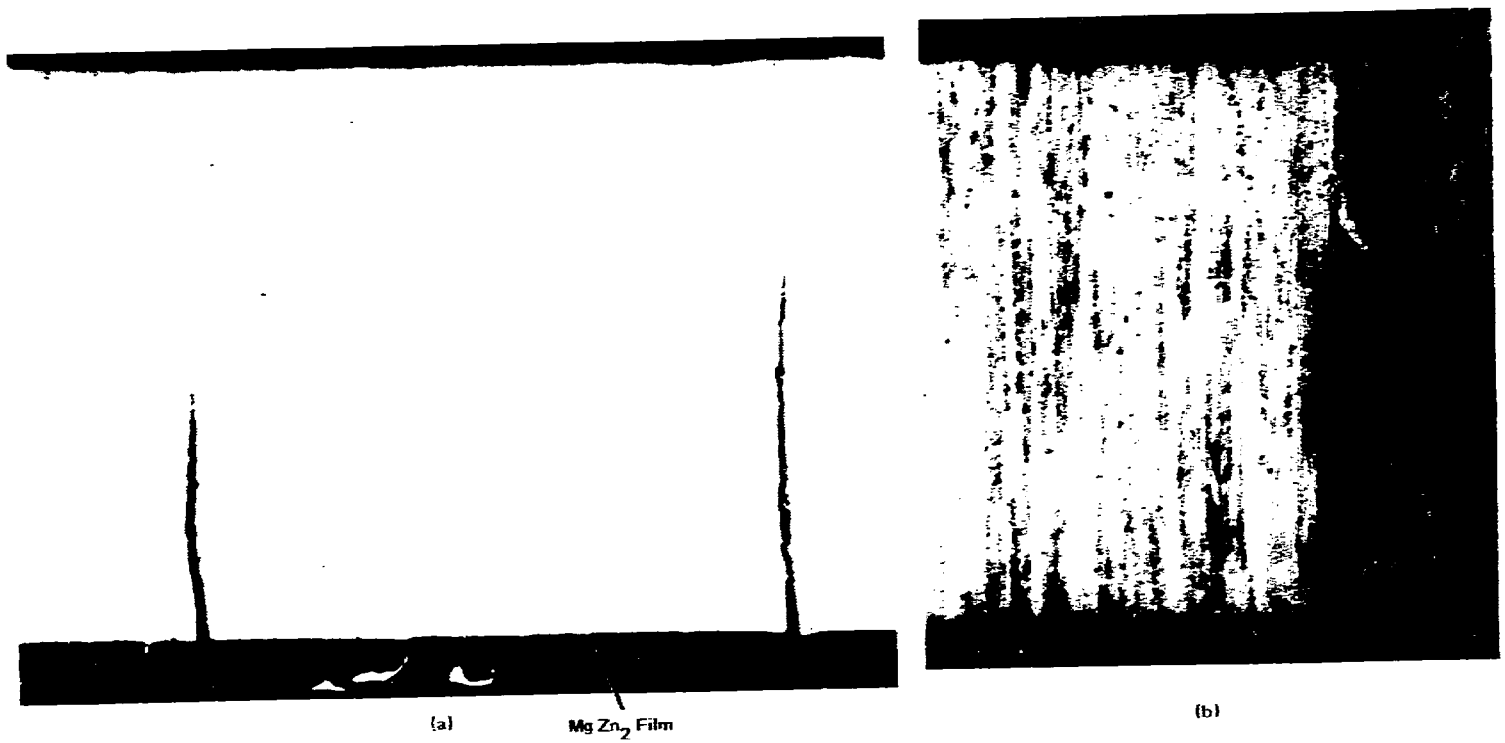

Fig. 7 Stress Corrosion Failure in $MgZn_2$ Film/Substrate Sample
(a) Intergranular Cracking Through 0.040-inch Thickness
(b) Etched Section Adjacent to Fracture Surface

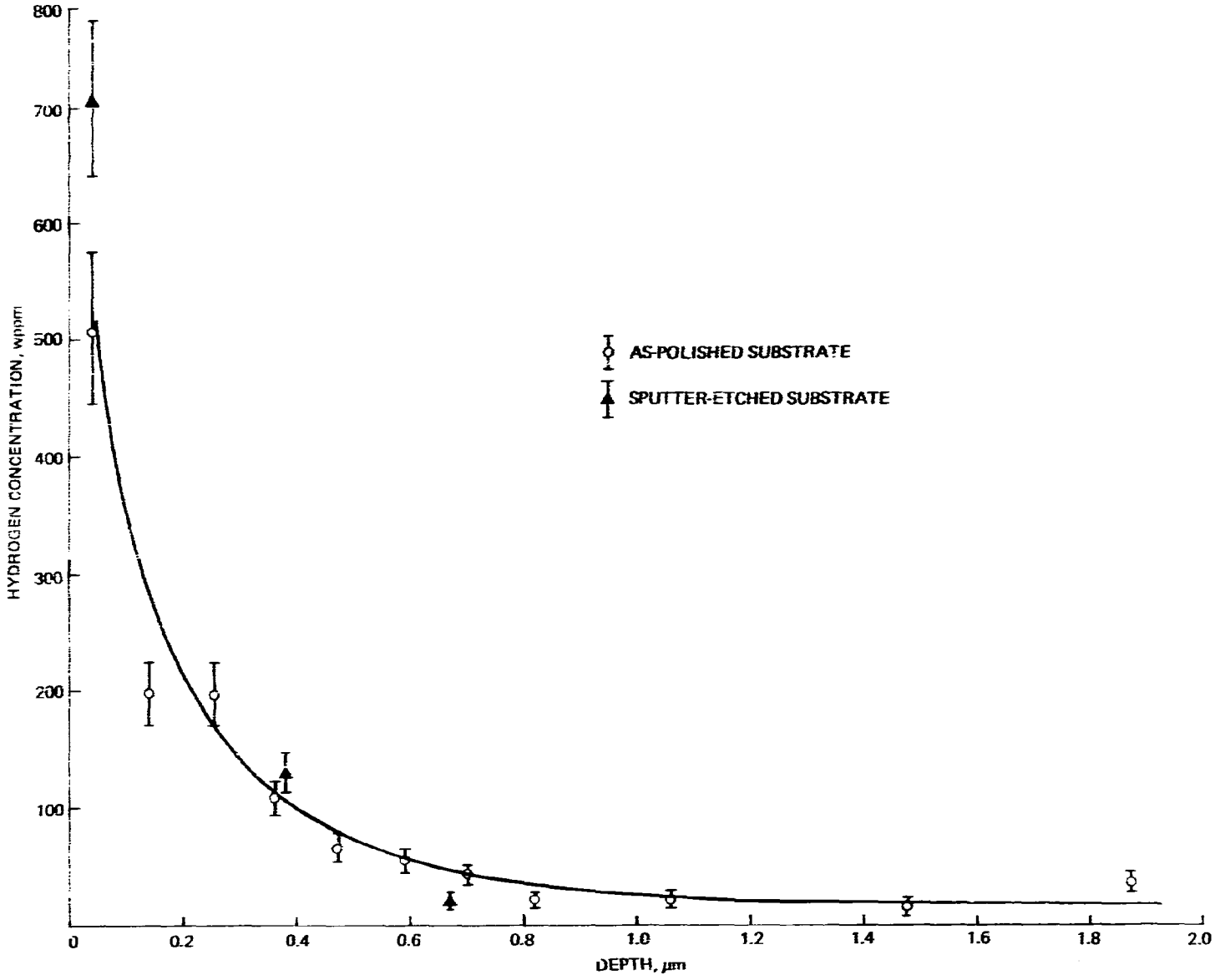

Fig. 8 Hydrogen Depth Profiles in 7075-T6 Substrate Surface

region is approximately 0.20 μm, a significant portion of the substrate surface volume is sampled. Therefore, the high hydrogen concentrations measured in the interface region appear to be directly related with the hydrogen concentration in the surface of the substrate.

Some explanation should also be given for the large differences in hydrogen concentration in the interface region between samples of the same condition. For example, concentrations of 121 ± 20 and 230 ± 32 wppm were measured in the interface region of two as-sputtered pure aluminum film/substrate samples. Throughout these measurements, a constant ^{7}Li beam energy of 4.75 MeV was utilized for determining the hydrogen concentration in the interface region. However, the film thickness of each sample differed so that the LNMH resonance reaction did not occur at the same position relative to the interface in all cases. As a result, the interface region sampled was not always comparable. Consideration of the effect of the relative position of the resonance energy on the hydrogen concentration is given in Table 7 for pure aluminum film/substrate samples. There appears to be no correlation between the relative position of the resonance energy and the measured hydrogen concentration. For the as-sputtered condition, a lower concentration was indicated when the resonance occurred in the substrate, whereas for stress corrosion under plastic loading, SCP, the reverse was true. In general, the variation in film thickness within the area probed, ± 0.06 mg/cm^2, coupled with the resonance width, averaged as ± 0.04 mg/cm^2, assured that the film, the singularity at the interface, as well as the substrate were sampled. However, because of this uncertainty it does not appear that the contribution of the separate sample volumes can be sufficiently resolved to explain the measured differences.

TABLE 7 POSITION OF RESONANCE ENERGY RELATIVE TO INTERFACE IN ALUMINUM FILM/SUBSTRATE SAMPLES*[1]

Condition	Film Thickness (mg/cm^2)	Δ*[2] (mg/cm^2)	Position of Resonance Energy	Measured Hydrogen Concentration (wppm)
S	0.79 ± 0.06	-0.12	substrate	121 ± 20
S	0.91 ± 0.06	0.00	interface	230 ± 32
C	0.95 ± 0.06	+0.04	interface	116 ± 20
C	0.92 ± 0.06	-0.09	substrate	85 ± 18
SCE	0.92 ± 0.06	+0.01	interface	189 ± 25
SCE	0.95 ± 0.06	-0.06	interface/ substrate	169 ± 24
SCP	0.79 ± 0.06	-0.12	substrate	229 ± 28
SCP	0.92 ± 0.06	+0.05	interface	123 ± 21

*[1] 0.91 ± 0.03 mg/cm^2 depth of resonance at 4.75 MeV

*[2] Δ = average film thickness - resonance energy depth

In connection with the lack of certainty in the position of the resonance energy, the method of determining the hydrogen concentration in the $MgZn_2$ film/substrate interface region will be described. To calculate the hydrogen concentration in wppm from the measured γ-ray count rate, the elemental constituency of the host material must be known, as indicated by the following (Ref. 16):

$$w_H = \left[1 + \frac{K \left[\frac{N}{Q} \right]^{-1} - \xi_H}{\sum_j \frac{M_H}{M_j} w_j^o \xi_j} \right]^{-1}$$

where w_H = hydrogen concentration

K = calibration constant

$\frac{N}{Q}$ = γ-ray count/unit charge

ξ_H = atomic stopping cross-section of hydrogen at resonance energy

M_H = atomic weight of hydrogen

M_j = atomic weight of species j

w_j^o = weight fraction of species j (without inclusion of hydrogen)

ξ_j = atomic stopping cross-section of species j at resonance energy

Because of the difficulty in resolving the position of the resonance energy in relation to the interface, the weight fractions of specific elements in the above equation could not be quantitatively identified. This was not a problem for the pure aluminum film/substrate and 7475 film/substrate samples because the difference introduced by using pure aluminum or the 7475 and 7075 alloys was relatively insignificant. For $MgZn_2$

film/substrate samples, a comparison is given in Table 8 between considering 100% $MgZn_2$ and 100% 7075 aluminum alloy for the same measured count rate, i.e., N/Q. As indicated, the concentrations for the 7075 aluminum alloy would be approximately 36 percent higher than for $MgZn_2$. Rather than assume that the reliability in the film thickness measurement was sufficient in each case to be used in calculating the concentration, a constant average concentration was utilized. In this way, the hydrogen concentration is a direct reflection of the measured count rate, N/Q, instead of a floating value that is dependent on the uncertainty in film thickness. The average values indicated in Table 8 are those used in Table 6.

Although the hydrogen concentration results in the interface region are limited by the number of samples examined and the extent of variation that exists, specific trends become apparent. These trends can be identified by considering the average hydrogen concentration in the interface, normalized to the as-sputtered condition, as shown in Table 9. No significant hydrogen enrichment is evident for any of the pure aluminum film/substrate exposures. In fact, there is a reduction in hydrogen concentration following corrosion exposure as well as accompanying removal of applied stress after stress corrosion exposure. No change occurs in the 7475 film/substrate interface following corrosion exposure, but increases of 26 and 40 percent are indicated for stress corrosion exposure under elastic and plastic loading, respectively. Upon removal of stress, the hydrogen concentration is reduced to the original level. For the $MgZn_2$ film/substrate interface, a decrease in hydrogen concentration, equivalent to that observed in the aluminum film/substrate interface, accompanies corrosion exposure. However, there is an increase of 34 percent following stress corrosion exposure under elastic loading, SCE, and a very large increase, greater than

TABLE 8 HYDROGEN CONCENTRATION EVALUATION FOR $MgZn_2$ FILM/SUBSTRATE INTERFACE REGION

Condition	Hydrogen Concentration (wppm)		
	Based on 100% $MgZn_2$	Based on 100% 7075	Average
S	181 ± 20	247 ± 28	214 ± 24
S	171 ± 20	234 ± 27	203 ± 24
C	118 ± 17	161 ± 23	140 ± 20
C	85 ± 14	116 ± 20	101 ± 17
SCE	231 ± 24	316 ± 33	274 ± 29
SCE	338 ± 34	462 ± 47	400 ± 41
SCE	143 ± 18	196 ± 25	170 ± 22
SCE-U	154 ± 19	211 ± 26	183 ± 23
SCE-U	386 ± 41	527 ± 56	457 ± 49
SCE-U	142 ± 18	193 ± 25	168 ± 22
SCP	360 ± 39	492 ± 54	426 ± 47
SCP-U	300 ± 32	410 ± 43	355 ± 38
SCP-U	455 ± 45	621 ± 62	538 ± 54

TABLE 9 COMPARISON OF AVERAGE HYDROGEN CONCENTRATION IN INTERFACE REGION

Condition	Normalized Hydrogen Concentration*[1]		
	Al Film/ 7075 Substrate	7475 Film/ 7075 Substrate	$MgZn_2$ Film/ 7075 Substrate
As-Sputtered (S)	1.00 (176 wppm)	1.00 (118 wppm)	1.00 (209 wppm)
Corrosion Exposure (C)	0.57	1.03	0.58
Stress Corrosion Elastic (SCE)	1.02	1.26	1.34
Unloaded SCE(SCE-U)	0.83	1.06	1.29
Stress Corrosion Plastic (SCP)	1.00	1.40	2.04*[2]
Unloaded SCP(SCP-U)	0.60	0.93	2.14 1.70*[2]

*[1] Normalized to indicated as-sputtered average concentration

*[2] Based on single sample

100%, associated with the stress corrosion exposure under plastic loading, SCP. Upon unloading, a reduction in hydrogen concentration occurred in one of the three SCE samples (see Table 6) and in the SCP sample that did not fail (indicated by asterisk in Table 9). Based on these observations, it appears that three levels of hydrogen enrichment accompany stress corrosion exposure:

1. No change - aluminum film/substrate (all exposures)
2. An approximate 30 - 40 percent increase -
   7475 film/substrate (SCE & SCP)
   $MgZn_2$ film/substrate (SCE)
3. An approximate 100 percent increase -
   $MgZn_2$ film/substrate (SCP)

In addition, unloading following stress corrosion exposure significantly reduces the existing hydrogen concentration in both aluminum film/substrate and 7475 film/substrate interfaces. Comparable reductions occur in the only half of the $MgZn_2$ film/substrate interfaces examined.

STRESS CORROSION MECHANISM

The intent of the present investigation was to determine whether the constituents at the grain boundary of high strength aluminum alloys had a preferential affinity for hydrogen when exposed to an aqueous chloride stress corrosion environment. If such an affinity exists, a hydrogen related mechanism that leads to the intergranular cracking characteristic of stress corrosion attack in these alloys can be inferred. Since direct measurement of the hydrogen concentration in the grain boundary region is not possible, a simulation was made to enable use of the LNMH technique in measuring the extent of the hydrogen

enrichment associated with stress corrosion exposure in grain boundary constituents and in the interface region between these constituents. Although the properties of the grain boundary state were not achieved by the sputtered film/substrate samples used in this simulation and the sputtered $MgZn_2$ films were not crystalline, control samples were utilized throughout to enable comparison and discern enrichment. Pure aluminum film/substrate samples provided comparison with a sample configuration that was not susceptible to stress corrosion attack, and the as-sputtered and corrosion exposure conditions served as a normalization for the stress corrosion exposure.

The results obtained in this investigation clearly show that hydrogen enrichment accompanies stress corrosion exposure in both 7475 film/substrate and $MgZn_2$ film/substrate interface regions. In addition, the extent of enrichment appears related to the magnitude of the applied stress for the $MgZn_2$ film/substrate interface. There was no indication of comparable increases in hydrogen concentration in either the film or substrate of any of the samples examined or in the interface region of the aluminum film/substrate samples. Moreover, the extent of enrichment was particularly high in $MgZn_2$ film/substrate interfaces and remained relatively high even when stress was removed. It appears that hydrogen diffused from the aqueous chloride solution into the interface region under the influence of stress and remained trapped when the solution environment was removed; for some of the $MgZn_2$ film/substrate samples, hydrogen remained trapped even after stress was removed.

Since stress corrosion cracking in high strength aluminum alloys has been shown to occur at the interface between a $MgZn_2$ grain boundary precipitate and the adjacent grain (Ref. 8) and

since the distribution of $MgZn_2$ grain boundary precipitates has been related with stress corrosion susceptibility (Refs. 11-15), the extent of hydrogen enrichment and trapping observed in the simulated $MgZn_2$/matrix interface of this investigation strongly suggests that hydrogen is of significance in the grain boundary embrittlement associated with stress corrosion.

Finally, it should be pointed out that two actual stress corrosion failures were encountered during this investigation. In both cases, failure occurred while stress alone was being maintained on $MgZn_2$ film/substrate samples following stress corrosion exposure. All substrates were susceptible to attack since they were prepared from 7075-T6 bar material and were stressed in their short transverse direction. However, only the two samples indicated underwent failure. It appears that the extend of hydrogen enrichment in the $MgZn_2$ film/substrate interface was of sufficient magnitude to cause attack in the substrate. These failures lend supporting evidence to the hypothesis that the extensive hydrogen enrichment at $MgZn_2$/ matrix interfaces which accompanies stress corrosion in an aqueous chloride environment promotes stress corrosion attack.

4. CONCLUSIONS

1. Use of a sputtered film/substrate sample configuration provides a suitable means for simulating the grain boundary constituency of 7000 series aluminum alloys.

2. There is significant hydrogen enrichment in the interface region of $MgZn_2$ film/substrate samples exposed to stress corrosion in an aqueous chloride solution; a lesser degree of enrichment occurs in the interface of 7475 film/7075 substrate samples; and no enrichment occurs in pure aluminum film/7075 substrate samples.

3. The extent of hydrogen concentration increase during stress corrosion exposure appears related to the magnitude of the applied stress.

4. The affinity for hydrogen in the simulated grain boundary interface between $MgZn_2$ and the matrix appears significant to the mechanism of stress corrosion attack in 7000 series aluminum alloys.

5. REFERENCES

1. Mondolfo, L.R., Metals Mater., Vol. 5, p. 95, 1971.
2. Ostermann, F. G. and Reimann, W. H., ASTM STP 467, p. 169, 1970.
3. Sprowls, D. O. and Brown, R. H., Metals Progr., Vol. 81, No. 4, p. 79, 1962.
4. Sprowls, D. O. and Brown, R. H., Metals Progr., Vol. 81, No. 5, p. 77, 1962.
5. Speidel, M. A., in Hydrogen in Metals, ed. by I. M. Bernstein and A. W. Thompson, ASM, p. 249, Metals Park, Ohio, 1974.
6. Green, J.A.S., Hayden, H. W., and Montague, W.G., in Effect of Hydrogen on Behavior of Materials, ed. by A. W. Thompson and I. M. Bernstein, TMS-AIME, p. 200, New York, 1976.
7. Gruhl, W. and Brungs, D., Metall., Vol. 23, p. 1020, 1969.
8. Montgrain, L. and Swann, P.R., in Hydrogen in Metals, ed. by I. M. Bernstein and A. W. Thompson, ASM, p. 575, Metals Park, Ohio, 1974.
9. Gest, R. J. and Troiano, A.R., Corrosion, Vol. 30, p. 274, 1974.
10. Sprowls, D.O. and Brown, R.H., Proc. of Conference on Fundamental Aspects of Stress Corrosion Cracking, ed. by R.W. Staehle, A. J. Forty, and D. van Rooyen, NACE, p. 498, Houston, Texas, 1969.
11. Adler, P. N., Delasi, R., and Geschwind, G., Met. Trans., Vol. 3, p. 3191, 1972.

12. Geschwind, G. and Adler, P.N., International Corrosion Conference - 73, Paper No. 97, NACE, Houston, Texas, 1973.

13. Unwin, P.N.T. and Nicholson, R.B., Acta Met., Vol. 17, p. 1379, 1969.

14. Kent, K.G., J. Aust. Inst. Metals, Vol. 15, p. 171, 1970.

15. Poulose, P.K., Morral, J.E., and McEvily, A.J., Met. Trans., Vol. 5, p. 1393, 1974.

16. Padawer, G.M., Adler, P.N., Kamykowski, E.A., Schneid, E.J., Kuehne, F.J. Jr., Stauber, M.C., and D'Agostino, M.D., "Development of a Nuclear Microprobe Technique for Hydrogen Analysis in Selected Materials," Final Report on NASC Contract N00019-72-C-0404, Grumman Research Department Report RE-464, Oct. 1973.

17. Padawer, G.M., Adler, P.N., and Stauber, M.C., "Further Development and Application of the Lithium Nuclear Microprobe for Hydrogen," Final Report on NASC Contract N00019-74-C-0176, Grumman Research Department Report RE-522, August 1976.

18. Adler, P.N., Padawer, G.M., and Kamykowski, E.A., Proc. of Tri-Service Corrosion of Military Equipment Conference, Vol. II, p. 25, AFML-TR-75-42, WPAFB, Dayton, Ohio, October 1974.

19. Adler, P.N., and Padawer, G.M., in Effect of Hydrogen in Behavior of Materials, ed. by A.W. Thompson and I. M. Bernstein, TMS-AIME, p. 698, New York, 1976.

20. Pearson, W.B., Lattice Spacings and Structures of Metals and Alloys, Peragamon Press, New York, 1958.

21. Guillet, L and LeRoux, R., in Intermetallic Compounds, ed. by J. H. Westbrook, P. 456, John Wiley and Sons, New York, 1967.

22. Whaling, W., The Energy Loss of Charged Particles in Matter, Handbuch der Physik, Springer-Verlag, Vol. 34, p. 193, 1958.

DISTRIBUTION LIST

(One copy unless otherwise noted)

(1 copy + balance after distribution)
Mr. E. Balmuth
AIR-52031G
Naval Air Systems Command
Washington, DC 20361

Commander
Naval Air Development Center
(Code 606)
Warminster, PA 18974

Naval Sea Systems Command
(Code 03423)
Department of the Navy
Washington, DC 20360

Naval Ships Research & Development
Center
(Code 2812)
Annapolis, MD 21402

Commander
Naval Surface Weapons Center
(Metallurgy Division)
White Oak
Silver Spring, MD 20910

Director, Naval Research Laboratory
(Codes: 6380, 6490, 6601, 8430 -
1 copy each)
Washington, DC 20390

Office of Naval Research
The Metallurgy Program, Code 471
Arlington, VA 22217

D.T.R. McNelley
Dept. of Mechanical Engineering
(Code 59)
Naval Postgraduate School
Monterey, CA 93940

14 Copies (12 copies for DDC,
2 copies for AIR-954)
Commander, Naval Air Systems Command
AIR-954
Washington, D.C. 20361

Wright-Patterson Air Force Base
Ohio 45433
Attn: W. Griffith, AFML/LLS

Wright-Patterson Air Force Base
Ohio 45422
Attn: C. L. Harmsworth, AFML/MXE

Army Materials & Mechanics
Research Center
Watertown, MA 02172
Attn: Dr. A. Gorum

Commanding Officer
Office of Ordnance Research
Box CM, Duke Station
Durham, North Carolina 27706

U.S. Army Armament R&D Command
(ARRADCOM)
Dover, NJ 07801
Attn: Dr. J. Waldman
DRDAR-SCM-P, Bldg. 3409

National Aeronautics & Space Administrati
Langley Research Center
Materials Division, Langley Station
Hampton, Virginia 23365
Attn: Mr. H. F. Hardrath
Stop 188M

National Aeronautics & Space Administrati
George C. Marshall Space Flight Center
Huntsville, Alabama 35812
Attn: Mr. J. G. Williamson
S&E-ASTN-MMC

National Academy of Sciences
Materials Advisory Board
Washington, D.C. 20418
Attn: Dr. J. Lane

Director
National Bureau of Standards
Washington, D.C. 20234
Attn: Dr. E. Passaglia

Battelle Memorial Institute
505 King Avenue
Columbus, Ohio 43201
Attn: Mr. Stephan A. Rubin, Mgr.
Information Operations

IIT Research Institute
Metals Research Department
10 West 35th Street
Chicago, Illinois 60616
Attn: Dr. N. Parikh

General Dynamics Convair Div.
P.O. Box 80847
San Diego, California 92138
Attn: Mr. Jack Christian, Code 643-10

Kaman Aerospace Corporation
Old Windsor Road
Bloomfield, Connecticut 06001
Attn: Mr. M. L. White

Rockwell International
Columbus Division
Columbus, Ohio 43216
Attn: Mr. P. Maynard, Dept. 75
Group 521

Rockwell International
Rocketdyne Division
Canoga Park, California 91305
Attn: Dr. Al Jacobs
Group Scientist
Materials Branch

Rockwell International
Los Angeles Division
International Airport
Los Angeles, California 90009
Attn: Gary Keller
Materials Applications

Lockheed Palo Alto Research Laboratories
Materials Science Laboratory
3251 Hanover Street
Palo Alto, California 94303
Attn: Dr. Frank A. Crossley
52-31/204

Lockheed California Company
P.O. Box 551
Burbank, California 91503
Attn: Mr. J. M. VanOrden
Dept. 74-71, Bldg. 221, Plt. 2

Lockheed-Georgia Company
Marietta, Georgia 30061
Attn: E. Bateh

Lockheed Missile & Space Corp.
Box 504
Sunnyvale, California 94088
Attn: Mr. G. P. Pinkerton
Bldg. 154, Dept. 8122
Mr. D.C. McIntyre
Bldg, 182, Dept. 84-13 (1 each)

Douglas Aircraft Company
3855 Lakewood Blvd.
Long Beach, California 90808
Attn: Mr. Fred Mehe, C1-250

Sikorsky Aircraft
Division of United Aircraft Corp.
Stratford, Connecticut 06497
Attn: Materials Dept.

Boeing-Vertol Company
Boeing Center
P.O. Box 16858
Philadelphia, Pa. 19142
Attn: Mr. J. M. Clark

The Boeing Company
Commercial Airplane
ORG. 6-8733, MS77-18
P.O. Box 3707
Seattle, Washington 98124
Attn: Cecil E. Parsons

Northrop Corporation
Aircraft Division
Dept. 3771-62
3901 West Broadway
Hawthorne, California 90250
Attn: Mr. Allen Freedman

Vought Corp.
P.O. Box 5907
Dallas, Texas 75222
Attn: Mr. A. Hohman

McDonnel Aircraft Company
St. Louis, Missouri 63166
Attn: Mr. H. J. Siegel
Materials & Processes Dev.
General Engineering Division

Lycoming Division
AVCO Corporation
Stratford, Connecticut 06497
Attn: Mr. Barry Goldblatt

Detroit Diesel Allison Division
General Motors Corporation
Materials Laboratories
Indianapolis, Indiana 46206

AiResearch Manufacturing Co. of America
Sky Harbor Aircraft
402 S. 36th St.
Phoenix, Arizona 85034
Attn: Mr. Jack D. Tree, Dept. 93-35-5M

General Electric Company
Aircraft Engine Group
Materials & Processes Technology
Laboratories
Evendale, Ohio 45215

Solar
2200 Pacific Highway
San Diego, California 92112
Attn: Dr. A. Metcalfe

Teledyne CAE
1330 Laskey Road
Toledo, Ohio 43601

Dr. Charles Gilmore
Tompkins Hall
George Washington University
Washington, DC 20006

Dr. Michael Hyatt
The Boeing Company
P.O. Box 707
Seattle, Washington 98124

General Electric Company
Corporate Research & Development
P.O. Box 8
Schenectady, New York 12301
Attn: Dr. D. Wood

Westinghouse Electric Company
Materials & Processing Laboratories
Beulah Road
Pittsburgh, Pennsylvania 15235
Attn: Don E. Harrison

Dr. John D. Wood
Associate Professor
Lehigh University
Bethlehem, Pennsylvania 18015

General Dynamics Corp.
Convair Aerospace Division
Fort Worth Operation
P.O. Box 748
Fort Worth, Texas 76101
Attn: Tom Coyle

Dr. A. I. Mlavsky
Senior Vice President for Technology &
Director of Corporate Technology Center
Tyco Laboratories, Inc.
16 Hickory Drive
Waltham, Massachusetts 02145

Martin Marietta Aluminum
Attn: Mr. Paul E. Anderson
(M/C 5401)
19200 South Western Avenue
Torrance, California 90509

Dr. Howard Bomberger
Reactive Metals, Inc.
Niles, Ohio 44446

Mr. W. Spurr
The Boeing Company
12842 72nd Ave., N.E.
Kirkland, Washington 98033

Dr. John A. Schey
Department of Materials Engineering
University of Illinois at Chicago Circle
Box 4348
Chicago, Illinois 60680

Rockwell International
P.O. Box 1082
1027 Camino Dos Rios
Thousand Oaks, California 91320

Pratt & Whitney Aircraft
Division of United Technologies
Florida Research and Development Center
P.O. Box 2691
West Palm Beach, Florida 33402

P. R. Mallory & Co., Inc.
3029 East Washington Street
Indianapolis, Indiana 46206
Attn: Technical Librarian

Martin Marietta Corporation
P.O. Box 5837
Orlando, Florida 32805
Attn: Dr. Richard C. Hall
Mail Point 275

Southwest Research Institute
8500 Culebra Road
P.O. Box 28510
San Antonio, Texas 78284
Attn: Dr. C. Gerald Gardner

Avco Space Systems Division
Lowell Industrial Park
Lowell, Massachusetts 01851

Brush Wellman, Inc.
17876 St. Clair Avenue
Cleveland, Ohio 44110
Attn: Mr. Bryce King

General Electric
Missile & Space Division
Materials Science Section
P.O. Box 8555
Philadelphia, Pennsylvania 91901
Attn: Technical Library

Kawecki Berylco Industries
P.O. Box 1462
Reading, Pennsylvania 19603

Linde Company
Division of Union Carbide
P.O. Box 44
Tonawanda, New York 14152

Midwest Research Institute
425 Volker Boulevard
Kansas City, Missouri 64110

University of California
Lawrence Radiation Laboratory
P.O. Box 808
Livermore, California 94550
Attn: Mr. L. W. Roberts

ERDA Division of Reactor Development
and Technology
Washington, D.C. 20545
Attn: Mr. J. M. Simmons, Chief
Metallurgy Section

Dr. W. C. Setzer, Director
Metallurgy & Surface Technology
Consolidated Aluminum Corp.
P.O. Box 14448
St. Louis, MO 63178

Kaiser Aluminum & Chemical Corp.
Aluminum Division Research Center
for Technology
P.O. Box 870
Attn: T. R. Pritchett
Pleasanton, CA 94566

Reynolds Metals Company
Metallurgical Research Division
4th and Canal Streets
Richmond, VA 23219
Attn: Dr. J. H. Dedrick

The Dow Metal Products Company
Hopkins Building
Midland, MI 48640

Dr. F. N. Mandigo
Olin Metals Research Laboratories
91 Shelton Avenue
New Haven, CT 06515

General Electric Co.
Corporate Research & Development
Bldg. 36-441
Schenectady, New York 12345
Attn: Dr. J. H. Westerbrook, Manager
Materials Information Services

Dr. E. A. Starke, Jr.
School of Chemical Engineering & Metallurgy
Georgia Institute of Technology
Atlanta, GA 30332

Dr. R. Balluffi, Chairman
Dept. of Materials Science & Engineering
Bard Hall
Cornell University
Ithaca, N.Y. 14853

Dr. D. J. Duquette
Materials Engineering Dept.
RPI
Troy, N.Y. 12181

United Technologies Research Laboratories
East Hartford, CT 06108
Attn: Mr. Roy Fanti

Autonetics Division of Rockwell
International
P.O. Box 4173
Anaheim, CA 92803
Attn: Mr. A. G. Gross, Jr.
Dept. 522-92